Wei, C. and Au, W. and Ketten, D. and Vishnu, H. and Ho, A.Z.H. 2019. Sound propagation in the near and far-field of a broadband echolocating dolphin and a narrowband echolocating porpoise, in Proceedings of the Fifth International Conference on the The Effects of Noise on Aquatic Life, Jul 7-12 2019. Den Haag, The Netherlands: Acoustical Society of America.

1. INTRODUCTION

Research into odontocetes biosonar beam measurement has shown that all odontocetes project a highly directional, relatively narrowed, and forwarding biosonar beam through the forehead during echolocation despite the beam properties vary among the species. (Au, 1993). The beam pattern of the animal's biosonar can be modeled by a circular piston radiator (Au et al., 1978). For a focused biosonar beam, the beam converges to a focal point or a focal region, then diverges, as shown in Fig 1a. However, if the beam doesn't converge to a focal point or a focal region with increasing distance, then it is an unfocused biosonar beam, as shown in Fig. 1b. Recent experiments regarding "melon focusing hypothesis" have led to different results. The latest discussion of the melon focusing hypothesis was proposed by Kloepper et al. (2012; 2015) who suggested that the biosonar beam emitted by a false killer whale (*Pseudorca crassidens*) was actively focused depending on target distance during target detection. While recent experiments examined the beam focusing property by measuring the biosonar beam of two *Tursiops truncatus* by Finneran et al. (2016) with a hydrophone array consisting of 45 elements arranged to two basic geometries. They measured the horizontal acoustic fields radiated from two dolphins when detecting targets at different distances and found no evidence of adaptive focusing in the near-field or far-field. After the examination of the data from Kloepper et al. (2015), Finneran et al. (2016) suggested that the reason for the discrepancy between the two results was likely a misinterpretation of data rather than a difference in biosonar emissions across species. The results from both studies represent the biosonar beams projecting in the horizontal plane. No measurements have examined this "melon focusing hypothesis" in the vertical plane. Previous studies have experimentally and numerically shown that the dolphin's elongated rostrum (with a dense bony structure) functions as an acoustic reflector in the formation of biosonar beam in the vertical plane (Aroyan et al., 1992; Houser et al., 2004; Finneran et al., 2014; Cranford et al., 2014, Wei et al., 2016, Wei et al., 2017; Wei et al., 2018a), whereas the air sacs covers most region of the bony structure in the nasal passages in the horizontal plane. Therefore, it is not known whether this significant structural difference would cause any variation in terms of the biosonar beam focusing property.

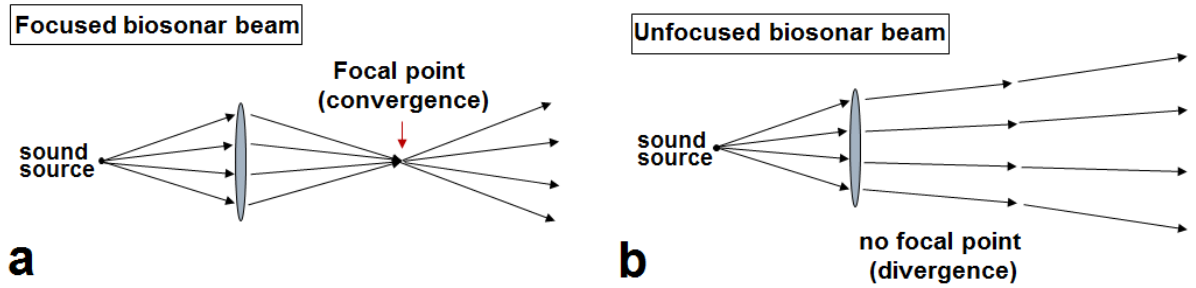

Figure 1. Schematic diagrams of the difference between the focused biosonar beam (a) and unfocused biosonar beam (b).

The biosonar signals emitted by odontocetes can be roughly classified into three broad categories: broadband high-frequency echolocation signals and narrowband high-frequency echolocation signals (Au et al., 1999; Au and Hastings, 2008; Au and Simmons, 2007) as well as frequency-modulated (FM) clicks (Madsen et al., 2005; Zimmer et al., 2005). Those species that use brief broadband echolocation clicks also tend to emit whistles. Among this category, bottlenose dolphin, beluga whale, and false killer whale are the most studied species. On the other hand, those species that produce narrowband high-frequency (NBHF) echolocation clicks usually do not emit whistles. Only a few species fall into this category; harbor porpoise is the best known of the non-whistling species. The beaked whale is the only species known to emit FM clicks, however, the acoustics of beaked whales have received minimal attention in regards to sound production and propagation and hearing characteristics. Although the broadband echolocation species and narrowband echolocation species seem to have a similar physical mechanism to excite vibration at the sound source to emit the biosonar signals, the characteristics of their biosonar signals are distinctly different.

In this study, finite element (FE) models were constructed to simulate the acoustic processes of an echolocation click emitted from the phonic lips in the animal's head propagating through the complex internal

structures and transmitted to the targets placed in the far-field. This type of numerical models has been applied to investigate the mechanism of echolocation emission and reception in some species of odontocetes (Aroyan et al., 1992; Aroyan, 2001; Cranford et al., 2014; Cranford et al., 2008; Wei et al., 2016; Wei et al., 2017; Wei et al., 2018a; Wei et al., 2018b). The techniques have led to significant advances in the understanding of internal acoustic processes and interactions associated with animals and surrounding media. The modeling data in this study visualized the sound propagation process from the near-field to far-field for an echolocating bottlenose dolphin and harbor porpoise in both horizontal and vertical planes. Additionally, the sound fields of the two species were obtained from the models to look for evidence of focusing on the click emission by plotting amplitude contours in both vertical and horizontal planes.

2. METHODS

A. NUMERICAL MODEL CONSTRUCTION

Computed tomography (CT) scanning is a non-invasive imaging technology that provides detailed anatomical geometry information for modeling construction. Both bottlenose dolphin and harbor porpoise specimen CT scan data were provided by Woods Hole Oceanographic Institution (WHOI) Biology Department. Approval from Institutional Animal Care and Use Committee (IACUC) for handling and examining the cadaveric specimens was granted by the Animal Use Committee of the Woods Hole Oceanographic Institution (WHOI) after reviewing the research protocol. Specimens scanned were obtained postmortem from freshly stranded animals under NMFS and NOAA permits to D.R. Ketten. The heads were scanned in prone position using a Siemens Volume Zoom helical CT scanner.

CT scans were conducted by using 1 mm spiral acquisition at 120 kV×125 mA and 120 kV×320 mA for *Tursiops* and *Phocoena*, respectively. Images were formatted in the transaxial plane at 0.1 to 1 mm slice increments. Raw acquisition data and all DICOM images were archived for both specimens. The data were imported into Software Mimics 10.1 Software (Materialise, Belgium) for analysis and three-dimensional (3D) geometrical model reconstruction (see Fig. 2). More details about the scanning and specimen can be found in Wei et al., 2018a and Wei et al., 2017, in which CT data was combined with animal tissue physical measurements to reconstruct acoustic impedance models for the heads of *Tursiops* and *Phocoena*, respectively. A slice closest to the midline that cut through the right phonic lips was selected to create the two-dimensional (2D) numerical model in the vertical plane for both specimens (Figs. 2a, c). For creating the horizontal models for both specimens, the slice which was on the animal's main beam axis and cut through the right phonic lips was extracted, as shown in Figs. 2b, d.

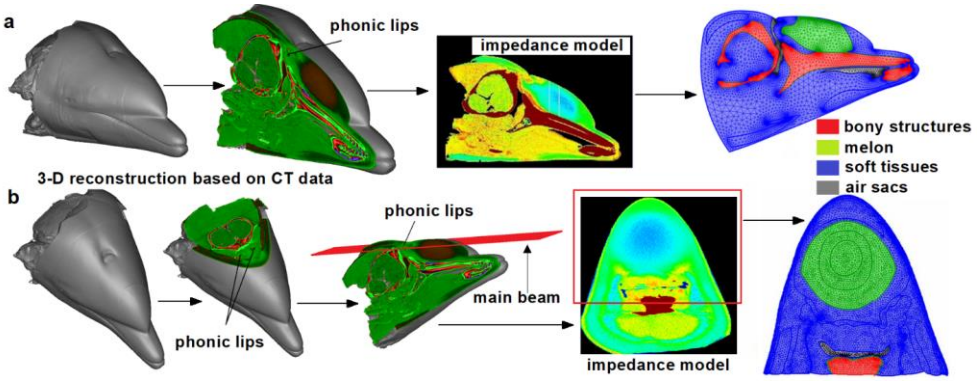

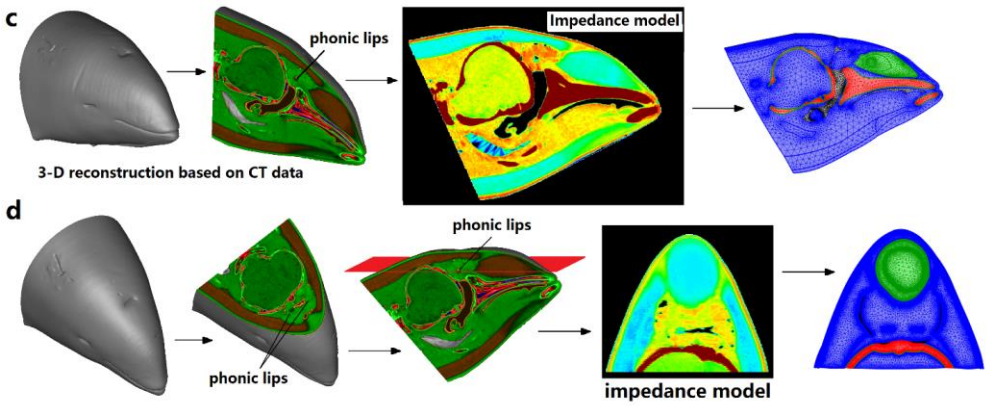

Figure 2. FE model reconstruction process

The reconstruction of the bottlenose dolphin sound propagation FE models in the vertical plane (a) and horizontal plane (b) and harbor porpoise sound propagation FE models in the vertical plane (c) and horizontal plane (d) based on high-resolution CT scan data.

B. FINITE ELEMENT MODEL CONSTRUCTION

The 2D impedance models were imported to COMSOL Multiphysics modeling software (Stockholm, Sweden) for finite element analysis and corresponding data analysis. Two types of FE models simulated the processes of the click emission and propagation from the interior biological structures to outside media in the vertical plane and horizontal plane, respectively. There were three main parts included in the FE models: the head of an echolocating dolphin or porpoise, the surrounding seawater, and a target. The structures included in the head of the animal for the two models differed based on the CT scan data. In the vertical FE model, the head of the animal contained structures such as the right side of phonic lips, melon, blubber, brain, musculature, mandibular fat, connective tissue, maxilla, mandible, vestibular sac, nasal passage, and premaxillary sac, etc. In the horizontal FE model, the head of dolphin included structures such as both sides of phonic lips, melon, connective tissue, musculature, cranium, vestibular sacs, and posterior nasofrontal sacs, whereas the head of the porpoise included such structures as both sides of the phonic lips, melon, connective tissue, musculature, cranium, brain, caudal sacs, and vestibular sacs. In order to simulate the process of target detection, an Polyvinyl Chloride (PVC) object was located in the far-field region. The object was placed at 1.2 m and 1 m from the sound source for *Tursiops* and *Phocoena*, respectively. For the different properties in tissues (e.g. blubber, muscle, mandibular fat, melon, connective tissue, and bony structures), the sound velocity and density values for the *Tursiops* were referenced to a previous study (Wei et al., 2018a), whereas the sound velocity and density values for *Phocoena* were referenced to Wei et al., 2017. For the media outside the animal's head, the sound velocity and density values of seawater and PVC material were set as 1483 m/s and 998 kg/m^3, 2380 m/s and 1380 kg/m^3, respectively.

In the simulation, the model was meshed into second-order triangular elements using COMSOL's free masher. The meshing layouts in the lateral view and polar view are displayed in Figs. 2. In order to obtain the solution with sufficient numeric precision, we performed the mesh refinement analysis for each model to choose the optimal element size. Finally, the element size for the model was set as at least ten elements per wavelength of the center frequency of the excitation signal at source ($\lambda = c_{water}/f$). The low-reflecting boundary condition (Bérenger, 1994) was applied to simulate the echolocation signal propagation in the free space.

Previous studies (Wei et al., 2017; Wei et al., 2018a) established FE models to simulate clicks emitted in the heads of a harbor porpoise and a bottlenose dolphin which then propagated from the near acoustic field to far acoustic field. Both models were confirmed and validated with actual biosonar signal measurements on the heads of live harbor porpoises (Au et al., 1999; Au et al., 2006; Koblitz et al., 2012) and bottlenose dolphins (Au, 1993; Au et al., 2010). The current work employed the same methods by performing the transient time domain finite element computation. The time steps of the models were set as 0.8 μs to obtain a very detailed sound propagation process. The type of the sound source was set differently for the model in the vertical and horizontal planes based on the CT scan data. According to the acoustic measurements results by Madsen et al. (2010; 2013), the right phonic lips are the site at which the echolocation clicks are generated. Consequently, the sound sources were placed at the right phonic lips in the models. In the sagittal section of the *Tursiops* CT scan data, the size

of the right phonic lips was approximately 3-4.5 mm, which was significantly smaller compared to the wavelength (1.85 cm) in the model. Thus a point source was suitable to model the source region for the FE model in the vertical plane. However, the size of the right phonic lips was approximately 30-33 mm in the axial sections (significantly longer than those on the left side). The length of the right phonic lips was much greater than the wavelength, therefore a line source was used in the FE model in the horizontal plane. In addtion, the driving signals for the two specimens were set differently. Wei et al. (2018a) suggested that the different driving sources could be one of the reasons causing different outgoing biosonar signals for broadband echolocation dolphin and narrowband echolocation porpoise. Therefore, in this study, a short-duration pulse with a broadband frequency characteristic was located at respective source locations of the *Tursiops* FE models as sound source excitations. In this case, the pulse can be written as in Eq. 1. An exponentially damped sinusoid with a narrowband frequency characteristic was employed at respective positions of the *Phocoena* FE models. For this case, the pulse can be written as in Eq. 2. The two types of pulses both simulate the phonic lips as open and closed immediately to generate a short pulse and subsequently attenuate afterward as the air pressure changes in the surrounding air sacs.

$$Q_m = -A^{-2\pi^2 f_0^2 (t-t_p)^2} sin(2\pi f_0 t), \quad t_p - \frac{1}{f_0} < t < t_p + \frac{1}{f_0} \tag{1}$$

$$Q_m = Aexp(\gamma t) sin 2\pi f_0 t \tag{2}$$

where A is the pulse amplitude (Pa), f_0 is the center frequency (Hz), t_p is the time from the onset of the signal to its peak amplitude (s), t is the time (s) and γ is the damping rate.

C. DATA ANALYSIS

The previous study of Finneran et al. (2016) arranged 45 hydrophones to form a rectangular configuration in a grid spanning the distances from -0.2 m to 0.2 m at the x axis and 0.2 m to 1 m at the y axis, with 0.1 m spacing between hydrophones. In order to compare the current study with these results and to examine also the focusing hypothesis proposed by Kloepper et al (2012; 2015) using FEA, 45 receiving points were located at the same positions as the hydrophones in the experiment of Finneran et al. (2016) that measured the transmitted signals from the near-field to far-field in the *Tursiops* horizontal plane. A similar idea was used to setup the *Phocoena* horizontal model. Because of the smaller head size, 35 receiving points were set in a rectangular configuration in a grid spanning the distances from -0.2 m to 0.2 m at x axis and from 0.15 m to 0.8 m at y axis. Since dolphins and porpoises both project their biosonar beam onto the rostrum, which differs in each species, the receiving points were located differently for the models in the vertical plane. The receiving points were set with a rectangular range from 0.4 m to 1 m at the x axis and from -0.1 m to 0.2 m at the y axis for *Tursiops*, and from 0.15 m to 0.8 m at the x axis and from -0.1 m to 0.2 m at the y axis for *Phocoena*.

The sound pressure fields in the vertical and horizontal planes were calculated. The sound pressure values were converted into dB scale (SPL $= \mathrm{A} + 20log_{10}P$), where P is the normalized peak-to-peak sound pressure of the received signal at each point and A is a constant. Origin Lab-OriginPro Software was used to plot the amplitude contour of the acoustic field and look for amplitude gain between the source and focal point (if it exists). Figs. 1b and d in the study of Finneran et al. (2016) plotted the contour patterns of a spherically focused baffled circular piston sound radiation and showing the contour of the focused beam. If the focusing exists, the contour would converge before the focal point and subsequently diverge beyond the focus distance. If the amplitude contour shows no sign of converging, such as the flat baffled circular piston sound radiation case in Figs. 1a and c in Finneran et al. (2016), then the sound beam is not focused and the melon focusing hypothesis is not true.

3. RESULTS AND DISCUSSIONS

To validate our models, some of the results from our FE models were compared to actual acoustic measurements on the live animals are shown in Fig. 3, which compares the acoustic near-field on the heads of the animals between simulated results (Wei et al., 2017; 2018a) and measurement results (Au et al., 2006; 2010). Figs. 3a, b were taken from Wei et al. 2017; 2018a and are shown here to facilitate our discussion. In the acoustic measurements, a suction cup hydrophone array was placed along the animal's forehead to record the outgoing biosonar signals. In our models, the receiving points were set at approximately the same positions as each hydrophone in the measurements. The relative amplitudes calculated from the two models clearly indicated that most energy in the outgoing beams was at the anterior portion of the forehead, where the region between points A to point B for both species. The simulated results coincided with the near-field acoustic measurement by Au et al. (2010) and Au et al. (2006). Fig.3b shows the comparison between the FE results and measured acoustic results regarding the waveform and its corresponding spectrum of the emitted biosonar signal directly in front of the two animals in the far-field. The similarity between the FE results and the measured results are clear. However, besides individual differences, it should be realized also that the signal generated by live animals are dynamic. There are slight variations from click to click, therefore the results represent only a qualitative comparison.

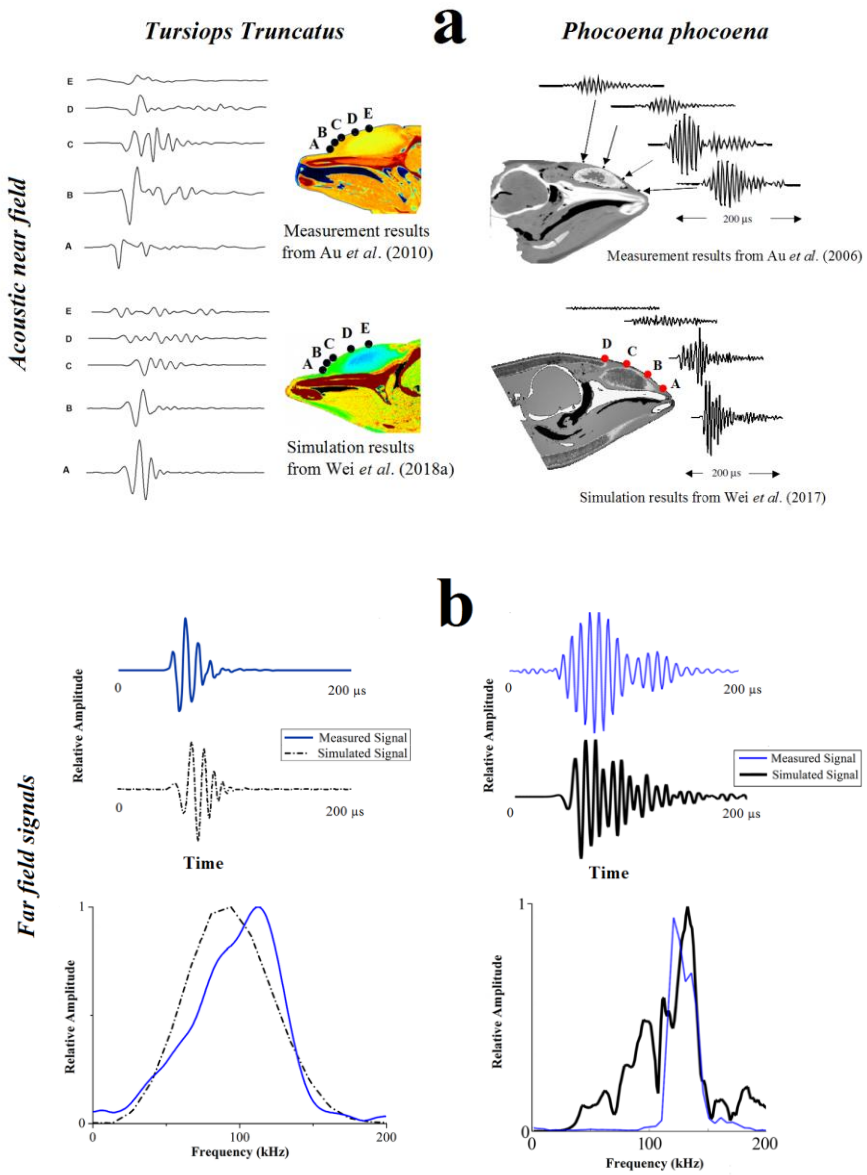

Fig. 3. Comparison between the simulated results and acoustic measurements results on the live animals.

(a) The received signals on the heads of animals in the near-field; (b) The waveforms and corresponding spectra of clicks received in the far-field.

The far-field beam patterns in both vertical and horizontal planes for an echolocating bottlenose dolphin from FE models were compared with the results from real acoustic measurements, as shown in Fig. 4. To plot the beam pattern, we set two receiving circles with a radius of 1.2 m and 1.1 m for the vertical plane and horizontal plane, respectively, where the peak-to-peak sound pressure of an echolocation click was determined. Au (1993) concluded that the average 3-dB vertical beamwidth from three bottlenose dolphins was 10.2°. Au et al. (1986) found that 89% of vertical beams had a major axis at 5°. In Fig. 4a, the major axis of the vertical beam was 5.3° above the x axis with an 11.1° 3-dB beamwidth, indicating the similarity between the simulated and measured results. In addition, the 3-dB beamwidth of the horizontal beam was 10.2 °, which was close to the measurement results averaged from different individuals (9.7°) (Au, 1993). The major axis of the horizontal beam from the FE model pointed towards -9.3 degrees to the left side. When we rotated the simulated horizontal beam to +10 degrees, the shape of the main beam from simulation better matched that of the measured one, as shown in Fig. 4b. The distorted internal structures (see Fig. 4c) might contribute to changing the direction of the sound propagation in the head. More discussion of this point as well as the contour results are given later in this paper.

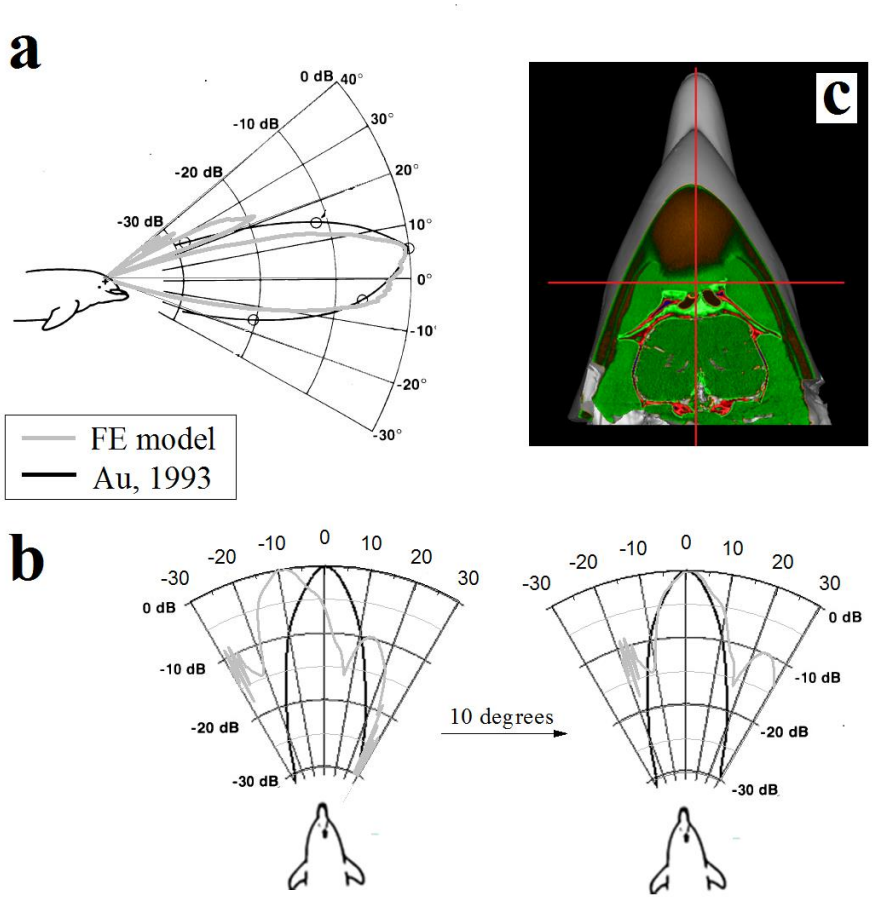

Fig. 4. Bottlenose dolphin far-field beam pattern.

Comparison of simulated beam pattern using FE models with actual measurements in the vertical (a) and horizontal (b) planes. The black curve represents the measured results by Au (1993) and the grey curve represents the simulated results from the FE model in this study. c. The asymmetrical internal structures may have led to deviation in the simulated horizontal beam pattern from the measured one.

For the harbor porpoise model, the receiving circle was placed with a radius of 0.9 m for both vertical and horizontal planes. Following the same procedure, we plotted the beam patterns for an echolocating harbor porpoise in both planes, as shown in Fig. 5. The beam pattern results were compared to two previous measurements by Au et al. (1999) and Koblitz et al. (2012) on different animals. In the vertical plane, the elevation of the simulated beam was 0.5° and the 3-dB beam width was 10.6°. Moreover, the elevation of the simulated horizontal beam was -4.9°, illustrating a high degree of agreement with measured results by Au et al. (1999), in which the major axis was pointed at approximately -5°. The simulated 3-dB beamwidth of the horizontal model in this study was 10.7°, which was lower than the measured beams from Koblitz et al. (2012) (13°) and Au et al. (1999) (16.5°). However, our vertical 3-dB beamwidth (10.6°) and horizontal 3-dB beamwidth (10.7°) were close, similar to the results from Au et al. (1999), in which the 3-dB beamwidths measured in both planes were both 16.5°. In general, in both vertical and horizontal planes, the simulated beams were relatively closer to the results measured by Koblitz et al. (2012) since the head sizes for the two animals were close. The diameter at the blowhole of the animal scanned in this study was 16.8 cm, which was close to that of the animal used in Koblitz's measurement (16.2 cm) but larger than that of the animal used in Au's measurement (14.8 cm). The width of the beam pattern is inversely proportional to the size of an animal's head.

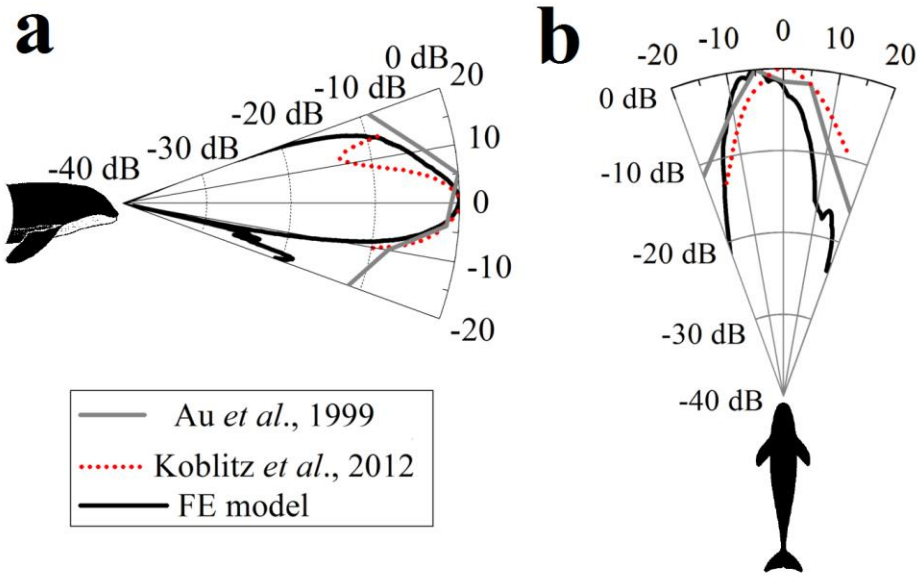

Fig. 5. Harbor porpoise far-field beam pattern.

Comparison of simulated beam pattern using FE models with actual measurements in the vertical (a) and horizontal (b) planes. The grey curve represents the measured results by Au et al. (1999), the dotted curve represents the measured results by Koblitz et al. (2012), and the black curve represents the simulated results from FE model in this study.

Noted that there are more side lobes contained in the beam patterns calculated by FEA for both species. One of the reasons could be the different spatial resolution between the measurements and FE models. In the previous acoustic measurements, the number of hydrophones used for recording the transmitted signals was limited. For example, Au et al. (1999) used 7 hydrophones in the experiments to measure the beam patterns; Koblitz et al. (2012) used 9 hydrophones and 8 hydrophones for the horizontal beam measurement and vertical beam measurement, respectively. Therefore, the spacing of the hydrophones was relatively large and the sensors were possibly too sparse to capture the undulations in the beam pattern. By contrast, in the beam pattern calculation using FEA, the spacing of each point was to 0.1 m, providing significantly finer spatial resolution for plotting the beam pattern and allowing us to capture the sidelobe fluctuations.

To look for the evidence of focusing in the biosonar signal propagation, an amplitude contour of the click propagation from the near-field to far-field in the horizontal plane was plotted and compared with the corresponding results experimentally measured by Finneran et al. (2016). The comparison results are shown in Fig. 6a. The black dots in Fig. 6a represents 45 receiving points which have the same positions as the 45

hydrophones placed in the measurements by Finneran et al. (2016). In Fig. 6a, the angle of the simulated primary projection axis towards the left, about 0.1 m away from the centerline at a distance of 1 m from the sound source. The maximum sound pressure region was between 0.2 to 0.5 m on the y axis, which was close to the maximum regions measured in the clicks emission of two live echolocating bottlenose dolphins (Finneran et al., 2016). The sound pressure in the far-field then steadily decreased with increasing distance. The characteristics of the acoustic field created by the click emission showed a close resemblance to that of a flat circular piston sound radiation. No converging patterns are observed in Fig. 6a, which is consistent with the measured results from Finneran et al. (2016) in Fig. 6b. The same procedure was used to obtain the amplitude contour for the harbor porpoise's biosonar beam in the horizontal plane, as shown in Fig. 6c. The maximum sound pressure region was between 0.15 to 0.25 m on the y axis, smaller than that of the bottlenose dolphin due to the smaller head size. The shape of the contour was similar to *Tursiops* contour measured by Finneran et al. (2016). No focal region or sign of convergence as mentioned in Kloepper et al. (2012; 2015) was found from the near-field to far-field. Therefore, our FE models provide no evidence of focusing for either broadband *Tursiops* or narrowband *Phocoena* in the horizontal plane.

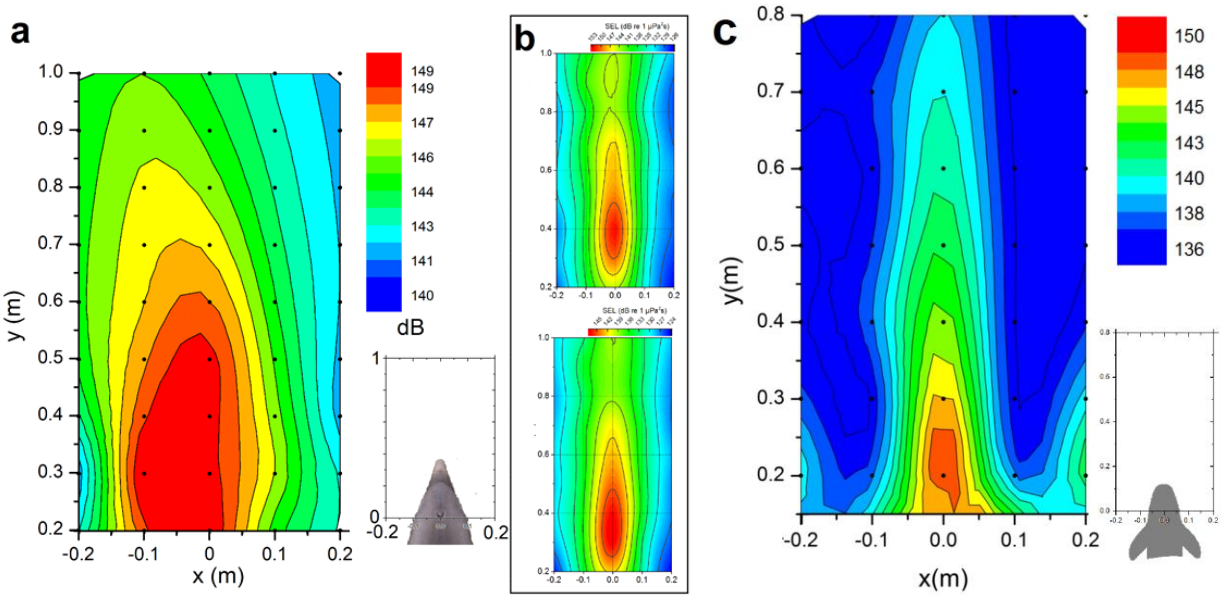

Fig. 6. Amplitude contours of two species in the horizontal plane.

Comparison of the horizontal amplitude contours between simulated results of this study (a) and measured results (b) of Finneran et al. (2016) from two live bottlenose dolphins. c. Horizontal amplitude contour of an echolocating harbor porpoise simulated by FE model. The black dots represent the positions of the receiving points.

The main axis of the simulated horizontal beam pattern in Fig. 4b was pointed to -9.3° and the simulated amplitude contour in the horizontal plane in Fig. 6a was also not symmetrical as well. Rather, the angle of the main axis was skewed to the left. Deviations of the main beam angle between the simulated amplitude contour and the measured one can be attributed to the CT data which was used to construct the numerical model. The carcass of the specimen had been kept frozen since the death of the animal. Before the CT scanning, we completely thawed the specimen in a water bath to ensure that the tissue acoustic properties were close to that of the live animals and carefully fixed the head on the motorized platform of the CT machine to avoid changing the shape of the head as much as possible. Nevertheless, gravity was still a factor and may have caused the internal structure in the head of the animal distorted somewhat (see Fig. 4c), resulting in an asymmetrical beam in simulation. A previous study (Moore et al., 2008) observed slight melon deformation in an echolocating dolphin and suggested that dolphins were able to steer the echolocation beam by varying the geometry of the internal structures. The maximum beam steering ability of the dolphin was calculated to be 18° in the horizontal plane. The horizontal sound propagation model of *Tursiops* in this study, and its deviation by a certain angle,

can be understood in a similar way as a case when a dolphin performs “beam steering” by slightly varying the geometry of the internal structures of its forehead. The slight deformation of the forehead results in an asymmetrical melon (Fig.4 c), causing the sound velocity gradient within the melon to change. Thus the sound propagation direction alters since the sound wave is guided along the lower acoustic impedance region when it propagates through the melon. The results further support the waveguide role of the melon proposed by Wei et al. (2017). Further, as another possible factor, the variation of the air sacs could cause the reflective surfaces to change, thereby altering the sound propagation direction by the sound being reflected by the inflated air sacs.

To further examine the focusing property for the vertical biosonar beam, the amplitude contour along the main beam axis of two species in the vertical plane was calculated following the same approach. The x axis was set at the rostrum of the animal. In Fig. 7, the maximum sound pressure region was in the distance at around 0.4 to 0.6 m from the sound source at the x axis for the *Tursiops* and 0.15 to 0.3 m for *Phocoena*, respectively. When the distance beyond the maximum region, both of the amplitudes of the acoustic pressure of the receiving signals varies as the inverse of the distance from the sound source. The contours in Figs. 7 distinctly showed the straightforward diverging sound propagation, indicating no converging behavior in either the near-field or far-field for both species.

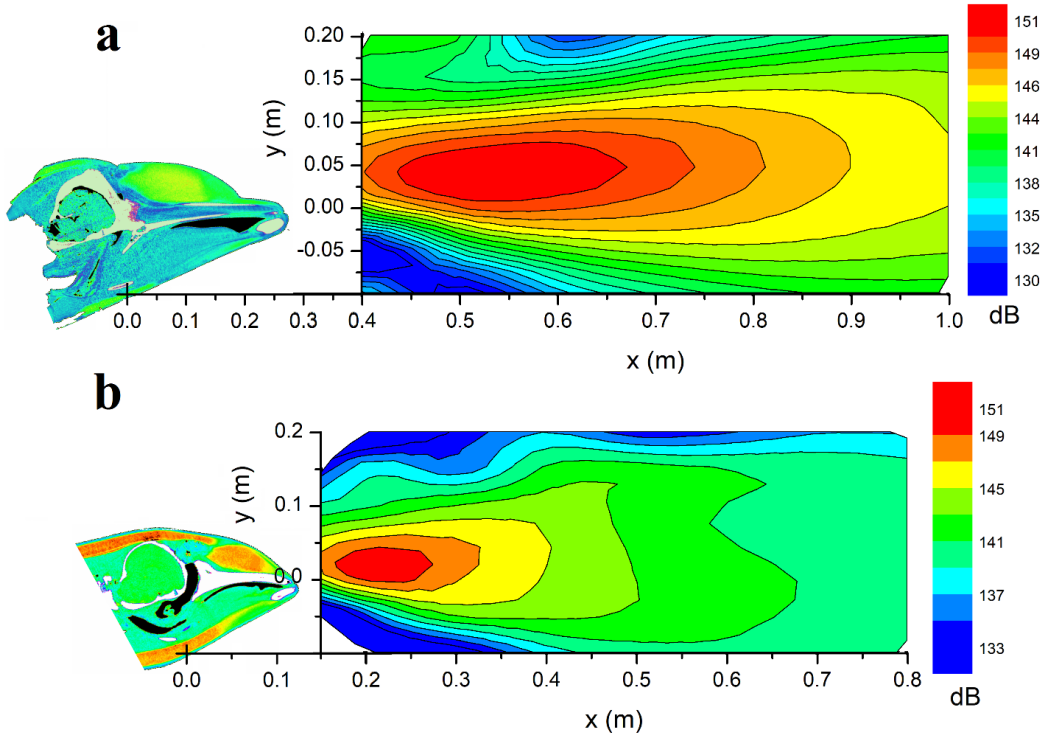

Fig. 7. The vertical amplitude contours of an echolocating bottlenose dolphin (a) and an echolocating harbor porpoise (b).

The previous study showed that the acoustic field of dolphin click emission can be approximated as the sound radiation from a flat circular piston with a radius from 4 to 5.7 cm (Au, 1993). The simulated amplitude contours in the vertical and horizontal planes (Figs. 6, 7) presented in this paper provide evidence to demonstrate the diverging characteristics of the outgoing biosonar beams in two species with the characteristics consistent with the radiation pattern of a flat circular piston. The data in the horizontal plane support the conclusion of the prior study by Finneran et al. (2016), where no evidence of focusing was found in the near-field and far-field.

The simulated vertical outgoing beams of the two species also demonstrate the diverging beam characteristics for two types of biosonar systems, indicating that the different characteristics of the clicks and head sizes and tissue configurations across the species cannot determine whether the biosonar beam is converging or diverging. For odontocetes, the combined effects of the complex internal structures in the heads

may be able to vary the outgoing beam properties (e.g. beamwidth, the angle of the main axis, etc.). However, our results based on our available resources indicate that the complex internal structures do not lead to creating a convergence in the biosonar beam. The odontocete biosonar beams are strongly directional but not focused. Therefore, the melon focusing hypothesis may not be accurate. It should be noted that the features and anatomic configurations of the internal structures in the heads of different odontocete species are different (Cranford et al., 1996), thus it is important to also examine the "melon focusing hypothesis" on other species.

Furthermore, Finneran et al. (2016) measured the acoustic fields when the position of the targets changed from 1.3 to 6.3 m. Due to the current computer power, in this study, the target in our model was located at a maximum distance of 1.2 m from the sound source. For the bottlenose dolphins, Au et al. (1978) measured that the transition between the acoustic the near-field and far-field exists from 0.5 m from the tip of the animal's rostrum. Therefore, as long as the acoustic field at the distance further than 0.8 m from the sound source can be considered to be in the far-field for bottlenose dolphins. Dolphin's click emission can be approximated based on the circular piston radiation theory. The sound pressure reaches the axial maximum at distance of a^2/λ, where a is the radius of the animal's head at the blowhole, λ is the wavelength of the signal. Thus, a harbor porpoise with the smaller head size results in the shorter distance of the near-field/far-field transition (less than 0.8 m). Thus, both of the models in this study can well represent the sound propagation from the acoustic the near-field to far-field for both species.

4. CONCLUSION

This study expanded the FE model to further examine the "melon focusing hypothesis" of the biosonar beam in the near-field and far-field by calculating the amplitude contours in both vertical and horizontal planes and looked for evidence of convergence. The data show that there was no evidence of convergence (no sign of focusing) in either the vertical plane or horizontal plane for the bottlenose dolphins, a typical broadband echolocation species. Additionally, the study also used a harbor porpoise FE model to demonstrate that a focal point or focal region does not exist for the narrowband echolocation porpoises, suggesting the same beam characteristics for two types of biosonar systems. The results help us gain a further visual understanding of the sound transmission in biosonar emission.

ACKNOWLEDGMENTS

One of the authors, Wei. C is supported by the fellowship from the Forrest Research Foundation. We are also grateful to Shuai Yang from Xiamen University, China, for the support of software and data analysis. Support for D. Ketten for this effort was provided by the Joint Industry Programme and by the Helmholtz Foundation.

REFERENCES

Aroyan, J. L. (2001). "Three-dimensional modeling of hearing in Delphinus delphis," J. Acoust. Soc. Am. 110(6), 3305-3318.

Aroyan, J. L., Cranford, T. W., Kent, J., Norris, K. S. (1992). "Computer modeling of acoustic beam formation in Delphinus delphis," J. Acoust. Soc. Am. 92(5), 2539-2545.

Au, W. W. L., Floyd, R. W., Haun, J. E. (1978). "Propagation of Atlantic bottlenose dolphin echolocation signals," J. Acoust. Soc. Am. 64, 411-422.

Au, W. W. L. (1993). "The Sonar of Dolphins," Springer-Verlag, New York.

Au, W. W. L., Hastings, M. (2008). "Principles of Marine Bioacoustics," Springer-Verlag, New York.

Au, W. W. L., Houser, D. S., Finneran, J. J., Lee, W., Talmadge, L. A., Moore, P. W. (2010). "The acoustic field on the forehead of echolocating Atlantic bottlenose dolphins (Tursiops truncatus)," J. Acoust. Soc. Am. 128(3), 1426-1413.

Au, W. W. L., Kastelein, R. A., Benoit-Bird, K. J. (2006). "Acoustic radiation from the head of echolocating harbor porpoise (Phocoena phocoena)," J. Exp. Biol., 209(14), 2726–2733.

Au, W. W. L., Kastelein, R. A., Rippe, T., Schooneman, N. M. (1999). "Transmission beam pattern and echolocation signals of a harbor porpoise (Phocoena phocoena)," J. Acoust. Soc. Am. 106(6), 3699–3705.

Au, W. W. L., Moore, P. W., Pawloski, D., (1986). "Echolocation transmitting beam of the Atlantic bottlenose dolphin," J. Acoust. Soc. Am. 80, 688-691.

Au, W. W. L., Simmons, J. A. (2007). “Echolocation in dolphins and bats,” Physics Today 60(9), 40-45.

Bérenger, J. P. (1994). “A perfectly matched layer for the absorption of electromagnetic waves,” Journal of Computational Physics 114(2), 185–200.

Cranford, T. W., Amundin, M., Norris, K. S., (1996). “Functional morphology and homology in the odontocete nasal complex: implications for sound generation,” J. Morphol, 228, 223-285.

Cranford, T. W., Krysl, P., Hildebrand, J. A., (2008). “Acoustic pathways revealed: Simulated sound transmission and reception in Cuvier's beaked whale (Ziphius cavirostris),” Bioinspiration & Biomimetics, 3(1):016001

Cranford, T. W., Trijoulet, V., Smith, C. R., Krysl P. (2014). “Validation of a vibroacoustic finite element model using bottlenose dolphin simulations: the dolphin biosonar beam is focused in stages,” Bioacoustics, 23(2), 161–194.

Finneran, J. J., Branstetter, B. K., Houser, D. S., Moore, P. W., Mulsow, J., Martin, C., and Perisho, S. (2014). “High-resolution measurement of a bottlenose dolphin's (Tursiops truncatus) biosonar transmission beam pattern in the horizontal plane,” J. Acoust. Soc. Am. 136(4), 2025-2038.

Finneran, J. J., Mulsow, J., Branstetter, B. K., Moore, P. W., and Houser, D. S. (2016). “Nearfield and farfield measurements of dolphin echolocation beam patterns: no evidence of focusing,” J. Acoust. Soc. Am. 140(2), 1346-1360.

Houser, D. S., Finneran, J. J., Carder, D. A., Van Bonn, W., Smith, C., Hoh, C., Mattrey, R., and Ridgway, S. H. (2004). “Structural and functional imaging of bottlenose dolphin (Tursiops truncatus) cranial anatomy,” J. Exp. Biol. 207(21), 3657-3665.

Kloepper, L., Buck, J. R., Smith, A. B., Supin, A. Y., Gaudette, J. E., Nachtigall, P. E. (2015). “Support for the beam focusing hypothesis in the false killer whale,” J. Exp. Biol. 218 (15), 2455-2462.

Kloepper, L., Nachtigall, P. E., Donahue, M. J., Breese, M. (2012). “Active echolocation beam focusing in the false killer whale, Pseudorca crassidens,” J. Exp. Biol. 215(8), 1306-1312.

Koblitz, J. C., Wahlberg, M., Stilz, P., Madsen, P. T., Beedholm, K., Schnitzler, H., (2012). “Asymmetry and dynamics of a narrow sonar beam in an echolocating harbor porpoise,” J. Acoust. Soc. Am. 131(3), 2315-2324.

Madsen, P. T., Johnson, M., Aguilar de Soto, N., Zimmer, W. M. X., Tyack, P. T. (2005). “Biosonar performance of foraging beaked whales (Mesoplodon densirostris).” J. Experimental Biology, 208, 181-194.

Madsen, P. T., Lammers, M., Winsniewaska, D., and Beedholm, K. (2013). “Nasal sound production in echolocating delphinids (Tursiops truncates and Pseudorca crassidens) is dynamic, but unilateral: clicking on the right side and whistling on the left side,” J. Exp. Biol. 216(21), 4091-4102.

Madsen, P. T., Wisniewska, D. and Beedholm, K. (2010). “Single source sound production and dynamic beam formation in echolocating harbour porpoises (Phocoena phocoena),” J. Exp. Biol. 213(18), 3105-3110.

Moore, P. W., Dankiewicz, L. A., and Houser, D. S. (2008). “Beamwidth control and angular target detection in an echolocating bottlenose dolphin (Tursiops truncatus),” J. Acoust. Soc. Am. 124(5), 3324–3332.

Norris, K. S., and Harvey, G. W. (1974). “Sound transmission in the porpoise head,” J. Acoust. Soc. Am. 56(2), 659-664.

Wei, C., Au, W. W. L., Ketten, D. R., Song, Z., Zhang, Y., (2017). “Biosonar signal propagation in the harbor porpoise's (Phocoena phocoena) head: The role of various structures in the formation of the vertical beam,” J. Acoust. Soc. Am. 141(6), 4179–4187.

Wei, C., Au, W.W. L, Ketten, D. R., Zhang, Y. (2018a). “Finite element simulation of broadband biosonar signal propagation in the near- and far-field of an echolocating Atlantic bottlenose dolphin (Tursiops truncatus).” J. Acoust. Soc. Am., 143, 2611-2620.

Wei, C., Au, W. W. L., Song, Z., Zhang, Y. (2016). “The role of various structures in the head on the formation of the biosonar beam of the baiji (Lipotes vexillifer),” J. Acoust. Soc. Am. 139(2), 875–880.

Wei, C., Song, Z., Au, W. W. L., Zhang, Y., Wang, D., (2018b). “A numerical evidence of biosonar beam forming of a neonate Yangtze finless porpoise (Neophocaena asiaeorientalis),” Journal of Computational Acoustics, 26, 1850009: 1-15.

Wei, C., Wang, Z., Song, Z., Wang, K., Wang, D., Au, W. W. L., Yu, Z. (2015). “Acoustic property reconstruction of a neonate Yangtze finless porpoise's (Neophocaena asiaeorientalis) head based on CT Imaging,” PLoS ONE 10(4), e0121442.

Wei, C., Zhang, Y., Au, W. W. L. (2014). “Simulation of ultrasound beam formation of baiji (Lipotes vexillifer) with a finite element model,” J. Acoust. Soc. Am. 136(1), 423–429.

Zimmer, W. M. X., Johnson, M. P., Madsen, P. T., Tyack, P. L. (2005). “Echolocation clicks of free-ranging Cuvier’s beaked whales (Ziphius cavirostrisi). J. Acoust. Soc. Am. 117, 3919-3927.